Engineering Uniform Nanocrystals: Mechanism of Formation and Self-Assembly into Bimetallic Nanocrystal Superlattices

Matteo Cargnello
Dept. of Chemistry, University of Pennsylvania, Philadelphia, PA 19104

Vicky V. T. Doan-Nguyen
Dept. of Materials Science and Engineering, University of Pennsylvania, Philadelphia, PA 19104

Christopher B. Murray
Dept. of Chemistry, University of Pennsylvania, Philadelphia, PA 19104

Dept. of Materials Science and Engineering, University of Pennsylvania, Philadelphia, PA 19104

DOI 10.1002/aic.15063
Published online October 14, 2015 in Wiley Online Library (wileyonlinelibrary.com)

The preparation of metal nanocrystals (NCs) with precise and tunable size is of great interest for many applications. Following previous reports on the synthesis of monodisperse nickel, palladium, and platinum NCs, we here show that the narrow size distributions are the result of an optimized combination of surfactants that play a dynamic, synergistic role in stabilizing the particles at different stages (nucleation, growth) of their preparation. This dynamical process allows the temporal separation of nucleation and growth responsible for the narrow size distributions achievable with this heat-up method. Finally, the uniform NCs are exploited in the preparation of binary nanocrystals superlattices entirely based on metal components, with promising applicability in the fields of catalysis, sensing, and optics. © 2015 American Institute of Chemical Engineers *AIChE J*, 62: 392–398, 2016
Keywords: nickel, palladium, platinum, surfactant, superlattice

Introduction

Nanocrystals (NCs) with precise tunability in size and shape in the 1–100 nm regime are of great scientific interest because of their properties that differ from bulk counterparts due to quantum-size effects.[1] This new class of materials has found application in several areas such as electronics and optoelectronics,[2–4] magnetics,[5] and catalysis.[6,7] These precisely tuned particles are not only scientifically interesting because of their novel properties, but can, in fact, provide valuable information on processes that occur at length scales where the transition between atomic or molecular and bulk properties plays a key role. Their precise structure allows us to investigate structure-property relations and thus, contribute to understanding the elements that lead to enhanced performance. In addition to the above elements, well-defined NCs provide the unique opportunity to exploit inexpensive self-assembly techniques for obtaining long-range ordered arrays where the position of the components is essentially dictated by entropy, opening new avenues for the design of inorganic materials at the molecular scale.[8] These assemblies of precise building blocks can occur in single component and in multicomponent mixtures, the latter structures known as binary nanocrystals superlattices (BNSLs). These arrays allow to study the collective properties that these novel systems show,[9,10] and have found use in describing particle-particle interactions.[11] The preparation of BNSLs entirely based on metals can be of great potential interest for catalytic applications as the proximity of two components with tailored size and interparticle distances can result in catalysts with improved activity and selectivity due to proximity effects or cascade reactions.

Various methods have been developed for the synthesis of monodisperse NCs in the case of semiconductor quantum dots,[12] metal,[13] and metal oxide particles.[14] These procedures often rely on postsynthesis treatments such as Ostwald digestive ripening[15] and size-selection procedures[12,16] to reduce the polydispersity of the sample or on complex procedures which involve injections that reduce the final yield of particles.[17] Few methodologies have been reported that are at the same time widely applicable and that do not rely on costly and time consuming selection processes to obtain monodisperse particles with reduced dimensions.[18,19] Understanding the path that these NCs take to form monodisperse samples is important to understand how to further tune their size, shape and composition, and to further engineer these structures at the atomic scale.

In this contribution, we show that the narrow size distributions in nickel (Ni), palladium (Pd), and platinum (Pt) NCs prepared by colloidal methods are a result of the role of different surfactants that stabilize the particles during their formation at

Current address of Matteo Cargnello: Department of Chemical Engineering and SUNCAT Center for Interface Science and Catalysis, Stanford University, Stanford, CA 94305

Correspondence concerning this article should be addressed to C. B. Murray at cbmurray@sas.upenn.edu.

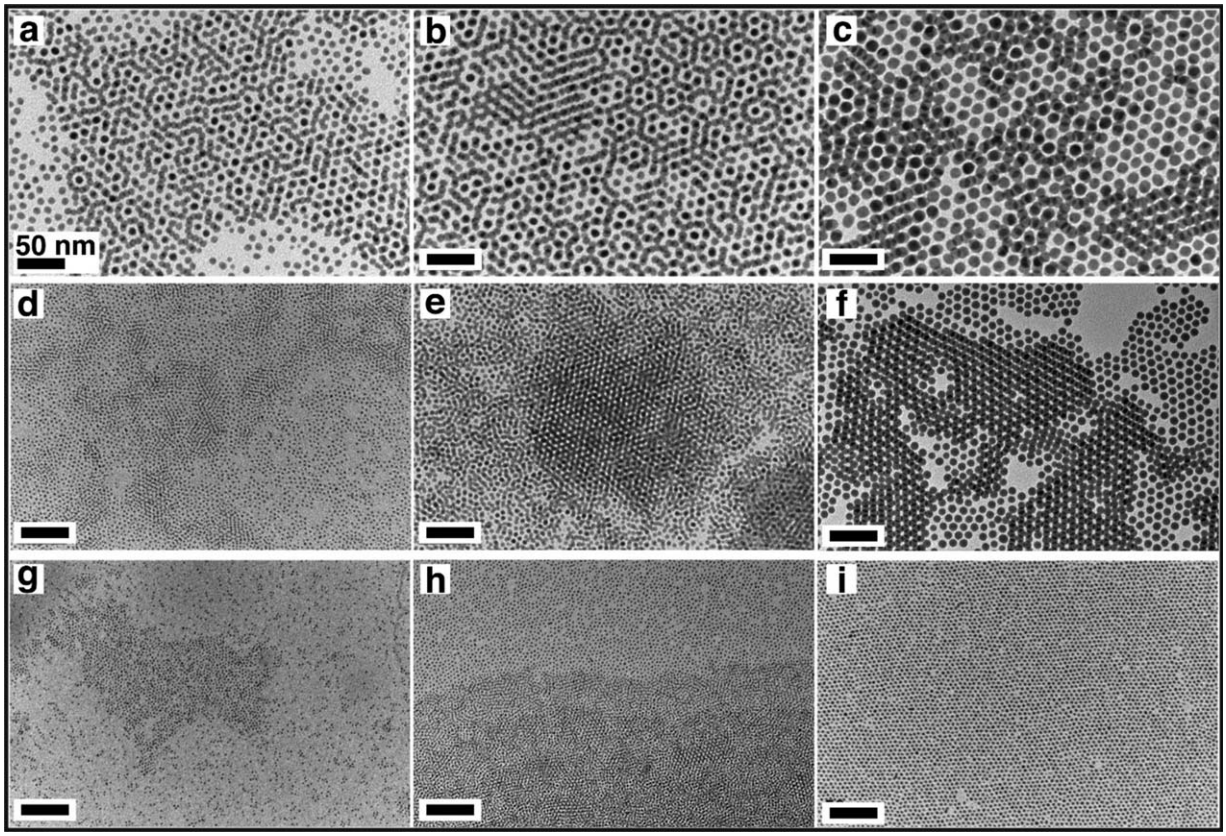

Figure 1. Ni (a, b, c), Pd (d, e, f), and Pt (g, h, i) NCs prepared with OLAM, TOP and eventually OLAC by high-temperature colloidal methods. The NC size increases from left to right in each series and it is related to the particular reaction conditions. All scale bars are 50 nm.

different stages (nucleation, growth, Ostwald ripening) of the synthesis. The size monodispersity of the NCs is further demonstrated by the preparation of different BNSLs based on the combination of two metals, which can be promising for catalytic and optical applications.

Experimental

Synthesis of Ni, Pd, and Pt particles

All synthesis were performed using standard Schlenk techniques following the procedures reported by Cargnello et al.[20] Briefly, Ni(II), Pd(II), or Pt(II) acetylacetonate salts were mixed with oleylamine (OLAM), trioctylphosphine (TOP), and eventually oleic acid (OLAC) in benzyl ether and the mixtures evacuated and heated to temperatures between 230°C and 290°C to allow the formation of NCs. To study the structural evolution of the NCs, aliquots of the reaction mixture (0.2 mL) were removed from the reaction flask at appropriate temperatures and quenched with isopropanol (5 mL), then NCs collected by centrifugation and redispersed in hexanes for characterization.

Assembly of nanoparticles into binary nanocrystal superlattices

Preparation of BNSLs followed published liquid-air interface assembly procedure.[21] Hexanes solutions of Ni, Pd, and Pt nanoparticles at approximately 3 mg mL^{-1} concentration were mixed in different volume ratios in a vial. A single drop of the mixed solutions was placed on the surface of diethylene glycol (DEG) in a Teflon well, the well was covered with a glass slide and left undisturbed to allow the slow evaporation of hexanes. BNSLs membranes were transferred to grids for transmission electron microscopy (TEM) by picking up the floating membranes from the subphase using tweezers and gently lifting up. Residual solvents (including DEG) were removed by further evacuation in a vacuum chamber under reduced pressure for at least 2 h.

Characterization techniques

TEM characterization was performed on a JEOL JEM-1400 microscope operating at 120 kV, and high-resolution TEM (HRTEM) characterization using a JEOL 2010F microscope operating at 200 kV. ^{1}H-, ^{13}C-, and ^{31}P-NMR (nuclear magnetic resonance) spectra were obtained at 25°C as $CDCl_3$ solutions on a Bruker DMX 300 operating at 300 MHz for proton.

Results and Discussion

Figure 1 summarizes NC samples that can be obtained with the method that we have been previously described.[20] Ni particles in the size range 3–12 nm, Pd in the range 2.5–6.3 nm and Pt in the range 2–3.7 nm can be obtained with size distributions below 6% without the need of any postsynthetic size-selective precipitation. The synthetic strategy involved the thermal decomposition of metal(II) acetylacetonate compounds in benzyl ether using OLAM, TOP, and OLAC as surfactants/stabilizing agents at different temperatures. In the case of Ni and Pd, mixtures of TOP and OLAM were sufficient to guarantee the isolation of monodisperse NCs of sizes above 2 nm. In the case of Pt, the addition of OLAC was necessary to grow larger (>2 nm) NCs. The size was tunable by

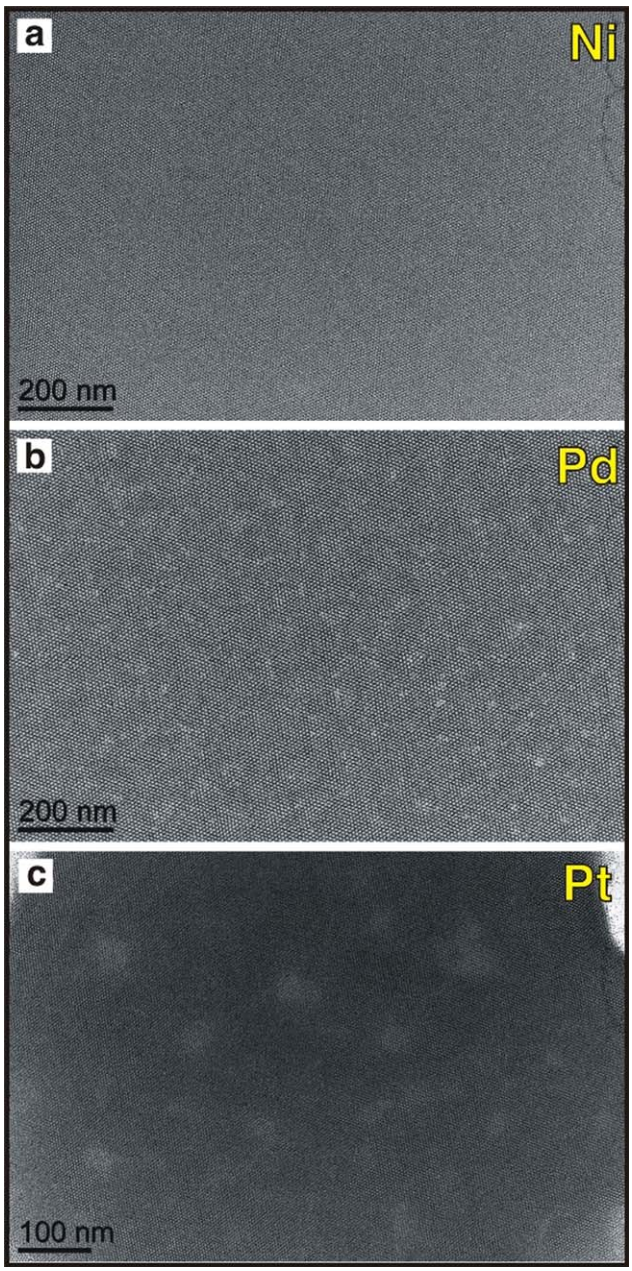

Figure 2. Representative TEM images showing the extended (up to μm) order of superlattices formed by (a) 3 nm Ni, (b) 6.3 nm Pd, and (c) 3.2 nm Pt monodisperse NCs.

[Color figure can be viewed in the online issue, which is available at wileyonlinelibrary.com.]

varying the temperature and/or the surfactants-to-metal ratio. The particles self-assembled into large patches of ordered superlattices even just by drop-casting concentrated solutions onto TEM grids (Figure 1). Using liquid-air self-assembly techniques, it was possible to obtain areas of superlattices that extended up to microns (Figure 2). The yields for all the procedures were quantitative when calculated based on the initial amount of acac precursors.

The formation mechanism of the uniform NCs was investigated using NMR. The nature of the precursor before any applied thermal treatment was studied in the case of Pd using correlated ^{31}P- and ^{13}C-NMR (Figure 3). The addition of OLAM to $Pd(acac)_2$ precursor (not shown) did not produce any change in the ^{1}H-NMR spectra indicating that the amine functionality was not able to displace the acac ligands in the Pd(II) coordination sphere. Conversely, when TOP was added in different ratios to $Pd(acac)_2$, a clear change in both the ^{13}C- and ^{31}P-NMR spectra was obtained. A TOP-Pd complex was formed as indicated by the appearance of new sets of signals in the ^{31}P-NMR spectra (between 20 and 30 ppm) and also by a change in the color of the solution from pale yellow to bright orange. The acac ligands were removed after the addition of two equivalents of TOP, as showed by the appearance of the signals of free acac ligand in the ^{13}C spectra at 202 ppm (Figure 3, right). The acac ligands were, therefore, removed from the coordination sphere, in contrast to what observed by Hyeon and coworkers.[16] However, only when four equivalents of TOP were added, a small signal belonging to free TOP in solution started to appear at −31 ppm. The formation of phosphine-Pd complexes at room temperature has been already demonstrated in the case of the reaction between Pd(II) acetate and triphenylphosphine,[22] as well as the reduction of Pd(II) centers to Pd(0), and the phosphine-Pd(0) adduct is unstable unless an excess of phosphine is used to stabilize the Pd(0) center. Therefore, it is reasonable to conclude that TOP immediately displaced acac ligands from $Pd(acac)_2$, forming a stable $Pd^{II}(TOP)_4$ complex. This complex may undergo reduction to Pd(0) in the presence of excess phosphine.[22] The formation of the Pd-TOP complex determines the formation of the true initial precursor, and because of the known equilibria involved in Pd-phosphine complexes, the addition of excess phosphine moves the equilibrium toward the tetracoordinated Pd, making the complex more sterically hindered and, therefore, more stable and harder to decompose with temperature. For this reason, we observed that the use of a large excess of TOP required very high reaction temperatures to induce the breaking of the TOP-Pd complex (Hyeon and coworkers performed the reaction at 300°C, Ref. 16), and working with near-stoichiometric amounts of phosphine allowed better tuning of the particle size.

OLAM was found to be a spectator at the initial stages of the synthesis. However, ^{1}H- and ^{31}P-NMR spectra of the final, purified Pd and Pt NCs demonstrated that only OLAM was present in the organic monolayer as protecting agent and that no signals related to phosphorus-containing compounds were present (Figure 4). High-performance liquid chromatography-mass spectrometry (HPLC-MS) analysis of the remaining washing solutions confirmed the presence of trioctylphosphine oxide (TOPO), in addition to unreacted OLAM. All of these elements combined provide evidence of a change in the coordination ligands of the growing Pd NCs and the replacement of TOP by OLAM occurring during the reaction. This process is not surprising considering that the starting Pd(II) ions have a soft character and prefer a soft coordinating base such as a phosphine. During the formation of Pd(0) NCs, however, the chemical hardness of the metal atoms determine the change in coordination to the harder amine base, and OLAM binds to the surface of the NCs.

To gain further insight into this process, we sampled the reaction at different stages (at 200°C, at 270°C, and after heating at 270°C for 10 min, whereas the final synthesis under these conditions requires to heat the precursors at 270°C for 15 min) and analyzed the particles after purification at each interval using TEM and NMR techniques with the results reported in Figure 5. The conditions used for this particular synthesis were: $Pd(acac)_2$ 0.5 mmol, TOP 2.5 mmol, OLAM 10 mmol, and 10 mL of benzyl ether. TEM images showed

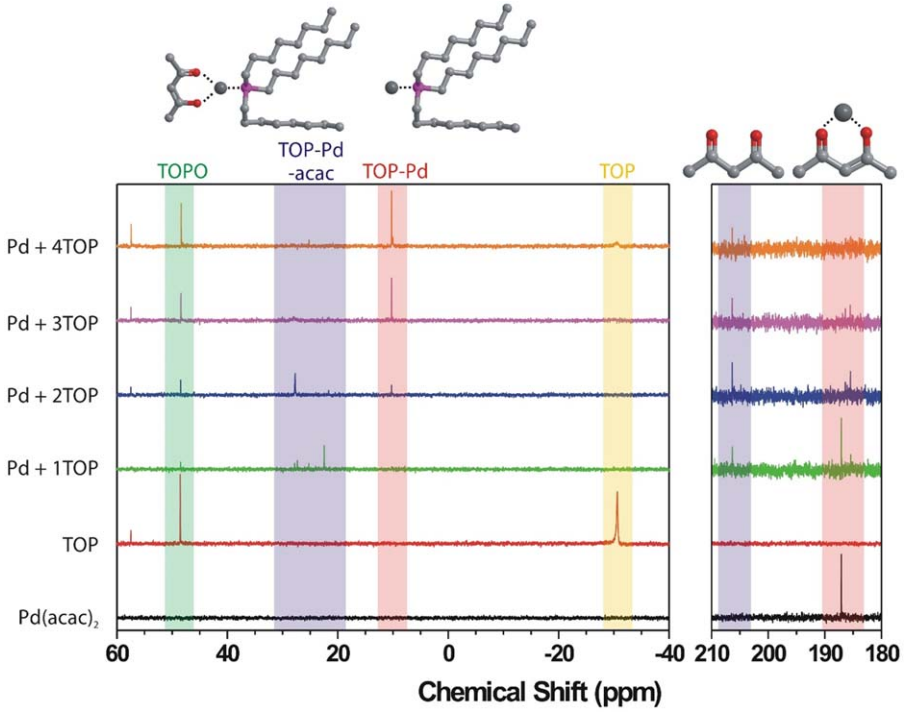

Figure 3. ^{31}P-NMR (left) and selected region of the ^{13}C-NMR (right) of the reaction between Pd(acac)$_2$ and multiple equivalents of TOP. The spectra of pure Pd(acac)$_2$ and pure TOP are reported for comparison.

[Color figure can be viewed in the online issue, which is available at wileyonlinelibrary.com.]

that at 200°C (Figure 5a) black spots were present on the grid, suggesting the presence of very small clusters that form agglomerates on the grid (the solution at this point was already black). At 270°C (Figure 5b) discrete Pd nanoparticles were clearly distinguishable, but size distribution was still polydisperse. After heating at 270°C for 10 min (Figure 5c) the average particle size increased and size distribution became narrower even if the value, 11%, was still higher than at the end of the synthesis (6%). Therefore, it is plausible that the growth of the particles follows an Ostwald ripening process in accordance with other procedures.[15,16] ^{31}P- and ^{1}H-NMR data indicated that the small clusters at 200°C were protected by TOP only. There was an absence of OLAM signal in the ^{1}H-NMR spectrum. When the temperature was increased to 270°C (Figure 5b), only a small fraction of TOP-Pd species remained, and OLAM-Pd species were the most abundant one detected in the ^{1}H-NMR spectrum. In the TEM image corresponding to this step of the synthesis, some very small particles/clusters were still visible. The data suggest that the growth of the particles started and TOP, being bulkier than OLAM, was replaced on the surface of the NCs probably due to steric effects. This trend was almost completed after heating the solution at 270°C for 10 min (Figure 2c), as at this point no signals related to phosphorus species were present in the ^{31}P-NMR spectrum and a ^{1}H-NMR spectrum resembling that of the final Pd particles was obtained. The presence of TOPO at the end of the reaction (as observed by HPLC-MS analysis) suggests that TOP is the reducing agent. The oxygen atoms needed for the oxidation of TOP to TOPO may derive from impurities present at the initial stages of the synthesis.[23]

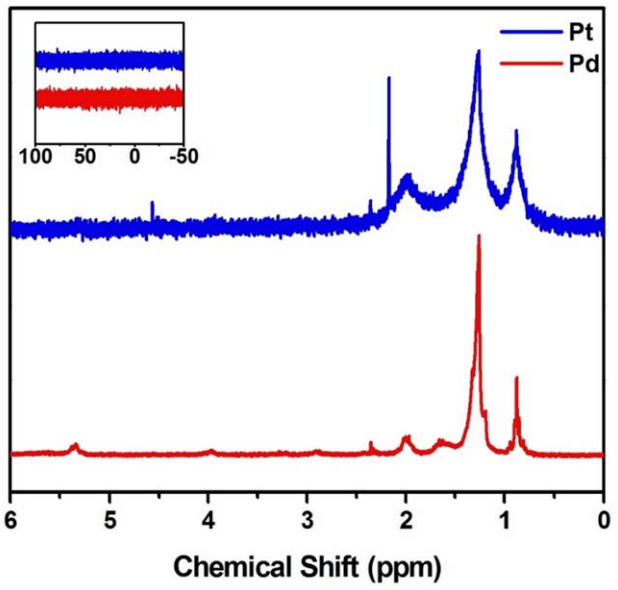

Figure 4. ^{1}H- and ^{31}P-NMR (inset) spectra of purified Pd and Pt nanoparticles showing the characteristic signals of OLAM in the ^{1}H spectrum and the absence of signals detected in the ^{31}P spectrum.

[Color figure can be viewed in the online issue, which is available at wileyonlinelibrary.com.]

The conclusions drawn for Pd can be extended to Ni and Pt. The different temperature windows required for the synthesis of the three metals (230°C for Ni, 250–290°C for Pd, and 300°C for Pt) were ascribed to the increased strength of the metal-TOP bond. Ni-TOP complex was found to decompose at lower temperatures than the corresponding Pd-TOP complex regardless of the excess of TOP and OLAM used.[24] On the contrary, the Pt-TOP complex was even more stable than Pd, being stable at temperatures ~300°C when the boiling

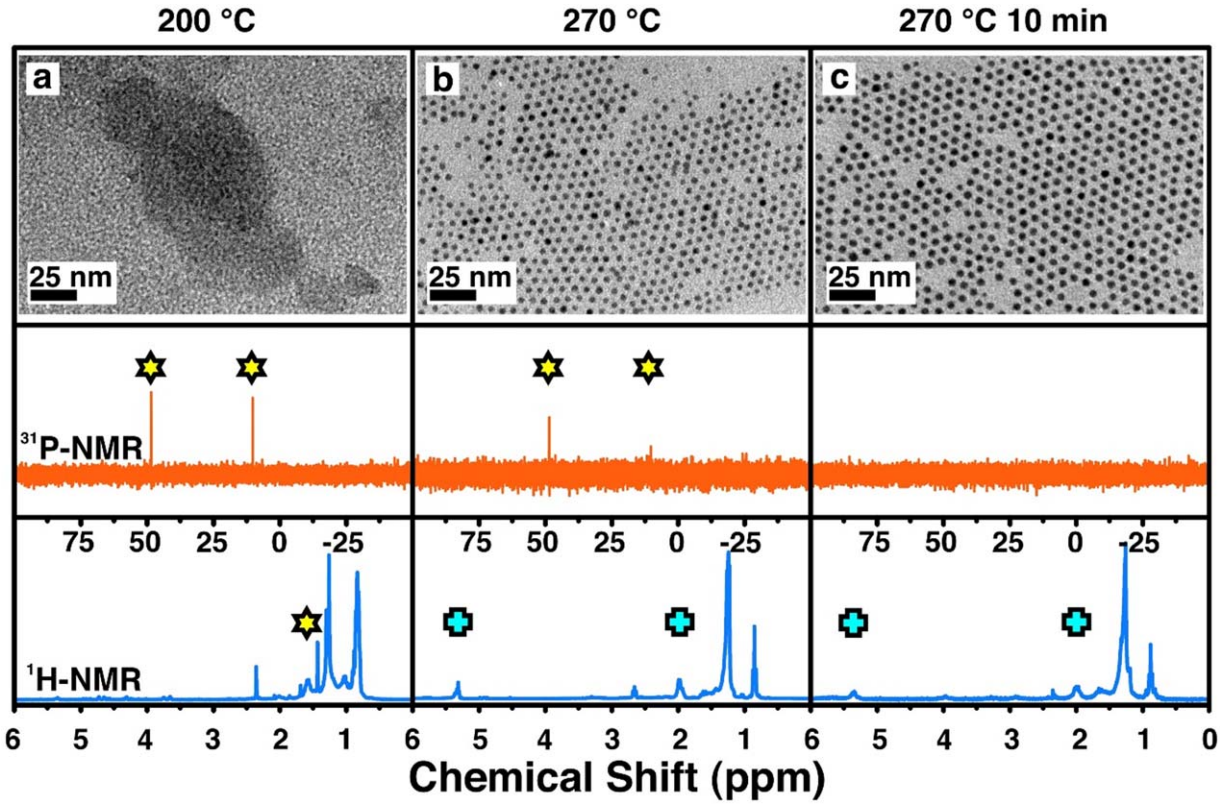

Figure 5. Representative TEM images (top), ^{31}P-NMR (middle), and ^{1}H-NMR spectra (bottom) of Pd nanoparticles at different stages of the reaction: 200°C (column a); 270°C (column b); after 10 min at 270°C (column c). Stars and crosses highlight NMR signals of TOP-Pd and OLAM-Pd species, respectively.

[Color figure can be viewed in the online issue, which is available at wileyonlinelibrary.com.]

point of the mixture was reached. We attribute this behavior to the increased π-back-donation from the metal to the 3d p orbitals as the electronegativity of the metal is reduced going from Ni to Pd to Pt. This element is in accordance with both theoretical and experimental studies.[25,26] In the case of Pt, the addition of OLAC was necessary to form larger NCs. The role of OLAC was peculiar in destabilizing the metal-TOP complexes. Its role is twofold: First, OLAC compete with TOP for the coordination to the metal center; second, the acid-base reaction between these two compounds could induce the formation of adducts that reduces the binding of TOP to form complexes with the metals. OLAC affected the various metals in different ways (Figure 6): while it resulted in the formation of large Ni structures of variable, faceted shapes, it promoted the formation of uniform and relatively larger (compared with when prepared without OLAC) Pd and Pt NCs. In the case of Ni, only large, faceted particles of different shapes and sizes were obtained, indicating that the addition of OLAC had a very strong effect on the growth of the Ni particles. This was due to the strong adsorption of OLAC on the Ni nuclei once these were formed, and likely to the fact that OLAC had a stronger binding to Ni than TOP. In the case of Pt, in a similar way, the presence of OLAC improved the decomposition of the metal precursor by reacting with TOP and reducing the temperature needed for the decomposition of the Pt-TOP complex. Finally, in the case of Pd, almost no effect was seen, as the particles were of similar dimension and size dispersion as those prepared in the absence of OLAC. This was due to the fact that the two effects, binding of OLAC directly to Pd and the reaction of OLAC with TOP, were balanced in strength in the case of Pd and the result was that similar characteristics of the particles were obtained. It is possible that further in-depth

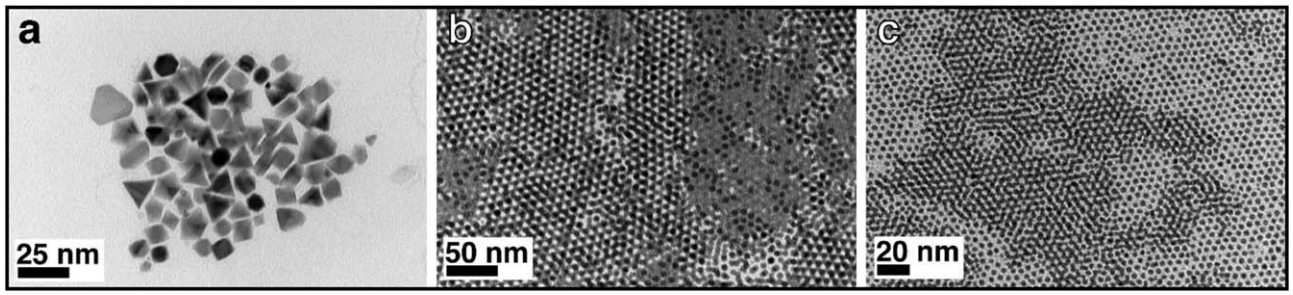

Figure 6. Effect of the addition of 20 equivalents of OLAC during the synthesis of (a) Ni, (b) Pd, and (c) Pt particles.

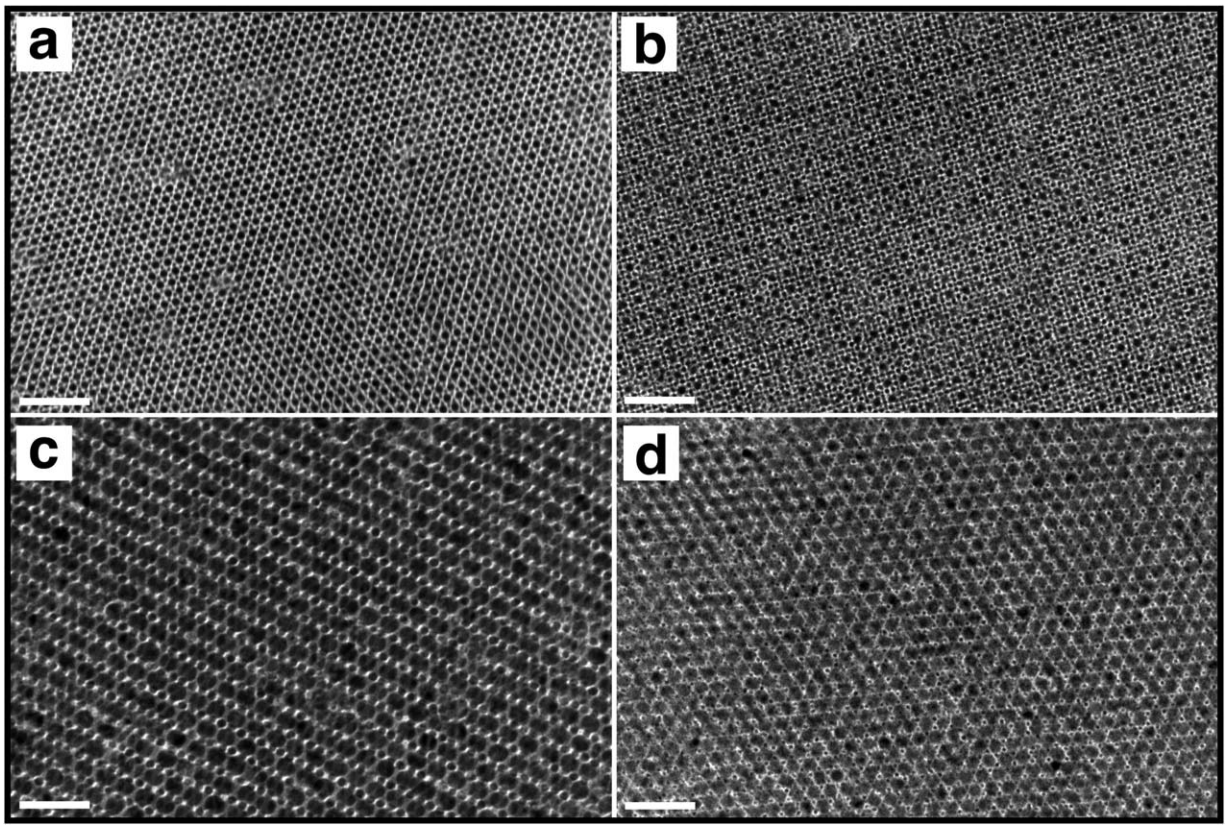

Figure 7. Binary nanocrystal superlattices self-assembled starting from the monodisperse NCs synthesized in this work (scale bars represent 50 nm).

(a) Pd-Pt AB_2-type BNSLs; (b) Pd-Pt AB_{13}-type BNSLs; (c) Pd-Ni AB_2-type BNSLs; (d) Pt-Ni NaCl-type BNSLs. Particles used are in this case 2.5 nm Pt, 6.3 nm Pd, and 12 nm Ni.

studies on the addition of OLAC to these syntheses can result in the preparation of faceted, anisotropic Ni particles and larger Pd and Pt NCs.

The monodispersity of the particles was finally exploited in the preparation of BNSLs based on the described Ni, Pd, and Pt particles. The variety of BNSLs prepared in this study is shown in Figure 7. AB_2, $AB_{13,}$ and NaCl-type systems were obtained. We calculated the effective size ratio γ between the two components, taking into account an average contribution of the OLAM capping molecules of 2 nm.[27] In the case of AB_2 systems, γ was $\sim$0.54 and $\sim$0.59 for Pt-Pd and Pd-Ni systems, respectively; for the Pd-Pt AB_{13}, γ was $\sim$0.54; and finally, for the Pt-Ni NaCl-type system, γ was $\sim$0.32. All these values are well in accordance with theoretical predictions based on optimum space filling.[28] The formation of AB_2 and AB_{13} systems starting from the same Pd-Pt nanoparticles was achieved using different concentrations of the two solutions. The preparation of BNSLs based entirely on metals is promising for catalytic or optical applications where the close proximity of two metallic surfaces can be advantageous as demonstrated by Kang et al.[11]

Conclusion

We reported here the study of the reaction mechanism for the formation of monodisperse NCs of Ni, Pd, and Pt. We showed that the ligands trioctylphospine and OLAM are synergistic in stabilizing the growing particles at different stages of the synthesis, guaranteeing an appropriate environment where nucleation and growth stages are separated and Ostwald ripening results in size dispersions below 6%. We also show the preparation of BNSLs using only metallic NCs as building blocks, with important perspectives for catalytic and optical applications.

Acknowledgments

Benjamin T. Diroll (University of Pennsylvania) is acknowledged for discussion. M.C. acknowledges primary support from the National Science Foundation through the Nano/Bio Interface Center at the University of Pennsylvania, Grant DMR08-32802. V.V.T.D.-N. acknowledges partial support for this work through Penn's NSF MRSEC under Award No. DMR-112090. C.B.M. is grateful for the support of the Richard Perry University Professorship.

Literature Cited

1. Kovalenko MV, Manna L, Cabot A, Hens Z, Talapin DV, Kagan CR, Klimov VI, Rogach AL, Reiss P, Milliron DJ, Guyot-Sionnest P, Konstantatos G, Parak WJ, Hyeon T, Korgel BA, Murray CB, Heiss W. Prospects of nanoscience with nanocrystals. *ACS Nano*. 2015;9(2):1012–1057.
2. Talapin DV, Lee JS, Kovalenko MV, Shevchenko EV. Prospects of colloidal nanocrystals for electronic and optoelectronic applications. *Chem Rev*. 2010;110(1):389–458.
3. Talapin DV, Murray CB. Applied physics: PbSe nanocrystal solids for n- and p-channel thin film field-effect transistors. *Science*. 2005; 310(5745):86–89.
4. Urban JJ, Talapin DV, Shevchenko EV, Kagan CR, Murray CB. Synergism in binary nanocrystal superlattices leads to enhanced p-type conductivity in self-assembled PbTe/Ag_2Te thin films. *Nat Mater*. 2007;6(2):115–121.

5. Sun S, Murray CB, Weller D, Folks L, Moser A. Monodisperse FePt nanoparticles and ferromagnetic FePt nanocrystal superlattices. *Science*. 2000;287(5460):1989–1992.
6. Lee H, Habas SE, Kweskin S, Butcher D, Somorjai GA, Yang P. Morphological control of catalytically active platinum nanocrystals. *Angew Chem Int Ed*. 2006;45(46):7824–7828.
7. Yamada Y, Tsung C-K, Huang W, Huo Z, Habas SE, Soejima T, Aliaga CE, Somorjai GA, Yang P. Nanocrystal bilayer for tandem catalysis. *Nat Chem*. 2011;3(5):372–376.
8. Shevchenko EV, Talapin DV, Kotov NA, O'Brien S, Murray CB. Structural diversity in binary nanoparticle superlattices. *Nature*. 2006;439(7072):55–59.
9. Murray CB, Kagan CR, Bawendi MG. Synthesis and characterization of monodisperse nanocrystals and close-packed nanocrystal assemblies. *Annu Rev Mater Sci*. 2000;30:545–610.
10. Talapin DV, Lee JS, Kovalenko MV, Shevchenko EV. Prospects of colloidal nanocrystals for electronic and optoelectronic applications. *Chem Rev*. 2009;110(1):389–458.
11. Kang Y, Ye X, Chen J, Qi L, Diaz RE, Doan-Nguyen VVT, Xing G, Kagan CR, Li J, Gorte RJ, Stach EA, Murray CB. Engineering catalytic contacts and thermal stability: gold/iron oxide binary nanocrystal superlattices for CO oxidation. *J Am Chem Soc*. 2013;135(4): 1499–1505.
12. Murray CB, Norris DJ, Bawendi MG. Synthesis and characterization of nearly monodisperse CdE (E = S, Se, Te) semiconductor nanocrystallites. *J Am Chem Soc*. 1993;115(19):8706–8715.
13. Park J, Joo J, Soon GK, Jang Y, Hyeon T. Synthesis of monodisperse spherical nanocrystals. *Angew Chem Int Ed*. 2007;46(25): 4630–4660.
14. Park J, An K, Hwang J, Park J, Noh H-J, Kim J-Y, Park J-H, Hwang N-M, Hyeon T. Ultra-large-scale syntheses of monodisperse nanocrystals. *Nat Mater*. 2004;3(12):891–895.
15. Stoeva S, Klabunde KJ, Sorensen CM, Dragieva I. Gram-scale synthesis of monodisperse gold colloids by the solvated metal atom dispersion method and digestive ripening and their organization into two- and three-dimensional structures. *J Am Chem Soc*. 2002; 124(10):2305–2311.
16. Kim S-W, Park J, Jang Y, Chung Y, Hwang S, Hyeon T. Synthesis of Monodisperse Palladium Nanoparticles. *Nano Lett*. 2003;3(9): 1289–1291.
17. Park J, Kang E, Son SU, Park HM, Lee MK, Kim J, Kim KW, Noh H-J, Park J-H, Bae CJ, Park J-G, Hyeon T. Monodisperse nanoparticles of ni and nio: synthesis, characterization, self-assembled superlattices, and catalytic applications in the Suzuki coupling reaction. *Adv Mater*. 2005;17(4):429–434.
18. Murray CB, Sun S, Doyle H, Betley T. Monodisperse 3d transition-metal (Co, Ni, Fe) nanoparticles and their assembly into nanoparticle superlattices. *MRS Bull*. 2001;26(12):985–991.
19. Hyeon T, Lee SS, Park J, Chung Y, Na HB. Synthesis of highly crystalline and monodisperse maghemite nanocrystallites without a size-selection process. *J Am Chem Soc*. 2001;123(51):12798–12801.
20. Cargnello M, Doan-Nguyen VVT, Gordon TR, Diaz RE, Stach EA, Gorte RJ, Fornasiero P, Murray CB. Control of metal nanocrystal size reveals metal-support interface role for ceria catalysts. *Science*. 2013;341(6147):771–773.
21. Dong A, Chen J, Vora PM, Kikkawa JM, Murray CB. Binary nanocrystal superlattice membranes self-assembled at the liquid-air interface. *Nature*. 2010;466(7305):474–477.
22. Amatore C, Jutand A, M'Barki MA. Evidence of the formation of zerovalent palladium from $Pd(OAc)_2$ and triphenylphosphine. *Organometallics*. 1992;11(9):3009–3013.
23. Li GY. The first phosphine oxide ligand precursors for transition metal catalyzed cross-coupling reactions: C-C, C-N, and C-S bond formation on unactivated aryl chlorides. *Angew Chem Int Ed Engl*. 2001;113(8):1561–1564.
24. Son SU, Jang Y, Park J, Na HB, Park HM, Yun HJ, Lee J, Hyeon T. Designed synthesis of atom-economical Pd/Ni bimetallic nanoparticle-based catalysts for Sonogashira coupling reactions. *J Am Chem Soc* 2004;126(16):5026–5027.
25. Pacchioni G, Bagus PS. Metal-phosphine bonding revisited. s-basicity, p-acidity, and the role of phosphorus d orbitals in zerovalent metal-phospine complexes. *Inorg Chem*. 1992;31(21):4391–4398.
26. Ahlquist MSG, Norrby PO. Dispersion and back-donation gives tetracoordinate [Pd(PPh3)4]. *Angew Chem Int Ed*. 2011;50(49):11794–11797.
27. Shevchenko EV, Talapin DV, Murray CB, O'Brien S. Structural characterization of self-assembled multifunctional binary nanoparticle superlattices. *J Am Chem Soc*. 2006;128(11):3620–3637.
28. Murray MJ, Sanders JV. Close-packed structures of spheres of two different sizes II. The packing densities of likely arrangements. *Philos Mag A*. 1980;42(6):721–740.

Manuscript received Aug. 11, 2015, and revision received Sep. 16, 2015.